ChemComm

COMMUNICATION

View Article Online
View Journal | View Issue

Cite this: *Chem. Commun.*, 2023, 59, 13607

Received 13th September 2023,
Accepted 23rd October 2023

DOI: 10.1039/d3cc04527g

rsc.li/chemcomm

In situ synthesis of rosette-like Co-doped FeNiOOH/NF for seawater oxidation†

Mingyuan Shi,[ab] Tianmi Tang,[b] Liyuan Xiao,[b] Jingyi Han,[b] Xue Bai,[b] Yuhang Sun,[ab] Yuanyuan Ma*[a] and Jingqi Guan *[b]

The development of high activity and strong resistance to seawater corrosion oxygen evolution reaction (OER) electrocatalysts for seawater electrolysis has broad application prospects. Herein, we prepare Co-doped FeNiOOH rosette-like nanoflowers on nickel foam (NF) with different Co dosages by one-step solvothermal method. The $Co_{0.2}$-FeNiOOH/NF exhibits a low overpotential (η_{10}) of 185 mV and Tafel slope of 30 mV dec^{-1} in 1 M KOH. Moreover, it shows a low η_{10} of 244 mV in alkaline seawater electrolyte. The remarkable OER performance of $Co_{0.2}$-FeNiOOH/NF is ascribed to the fact that the introduction of Co regulates the morphology and electron structure of the material, which provides abundant active sites for the reaction and promotes charge transfer. *In situ* Raman results demonstrate that NiOOH and γ-FeOOH are the key active species for the OER. This study provides a feasible basis for seawater electrolysis over transition metal (oxy)hydroxides.

Hydrogen is one of the most promising clean energy sources to solve fossil fuel depletion and environmental pollution[1,2] wherein, hydrogen production from electrolytic water has great development potential because of its advantages of unlimited raw material, cleanliness and high purity.[3,4] However, due to the four-electron reaction process involved in the OER,[5,6] the reaction kinetics is slow, and higher overpotential is required than that in the hydrogen evolution reaction (HER). Moreover, fresh water is mainly used for hydrogen production by water electrolysis at present, which greatly increases the production cost. Compared with limited fresh water resources, seawater accounts for approximately 97% of the total water volume,[7] and the geographical distribution is uniform. Therefore, seawater electrolysis has very important practical significance. However, the existence of Cl^- anions in seawater can result in chlorine evolution reaction (ClER) at the anode during electrolysis and the formation of hypochlorites, which will reduce the efficiency of seawater decomposition.[8] Therefore, it is particularly important to prepare OER catalysts with low cost, high activity and strong resistance to seawater corrosion.

In recent years, transition metal compounds (*e.g.*, nitrides,[9] phosphides,[10] hydroxides,[11] and (oxy)hydroxides[12]) have shown good OER performance. Among them, NiFe-based compounds stand out due to their advantages of high activity and adjustable three-dimensional electronic structure.[13] The real active centers of NiFe-based catalysts are metal (oxy)hydroxides.[14] Therefore, the direct synthesis of NiFe-based (oxy)hydroxides will have good OER activity. However, due to the poor electrical conductivity and weak adsorption capacity for oxygen-containing intermediates, further design is needed to overcome these shortcomings. At present, the strategies to improve the OER performance of transition metal (oxy)hydroxides mainly include regulating the electronic structure by introducing defects,[15] changing the morphology to produce more active sites,[16] and composite engineering to produce synergistic effects.[17] Heteroatom doping has attracted extensive attention because it can easily regulate the electronic structure of metal active sites, improve the conductivity and decrease the free energy of reactive intermediate species on the catalyst surface.[18,19] For example, Ding *et al.* synthesized W-doped NiFe-layered double hydroxide on carbon paper (CP),[20] which exhibited a low η_{10} of 239 mV in 1 M KOH. XPS spectra indicated that Fe 2p was negatively shifted after W doping, indicating that the electronic environment of Fe site was regulated. Lan *et al.* prepared Mo doped Ni_3S_2 (Mo-Ni_3S_2/NF) for seawater electrolysis.[21] In alkaline seawater, Mo-Ni_3S_2/NF needed an η_{10} of 212 mV. Due to the formation of NiOOH and sulfate ions during the reaction, the doping of Mo promotes the coordination of Ni-S, and thus the synthesized material has excellent catalytic activity and corrosion resistance.

In this work, we *in situ* synthesized Co-doped FeNiOOH/NF catalyst by the solvothermal method. As displayed in Fig. 1a, PVP as a structure directing surfactant was related to the

[a] *College of Chemistry and Chemical Engineering, Qiqihar University, Heilongjiang Province 161006, China. E-mail: mayuanyuan1219@126.com*
[b] *Institute of Physical Chemistry, College of Chemistry, Jilin University, Changchun 130021, P. R. China. E-mail: guanjq@jlu.edu.cn*

† Electronic supplementary information (ESI) available: Experimental details, XRD patterns, SEM images, OER polarization curves, and OER stability test. See DOI: https://doi.org/10.1039/d3cc04527g

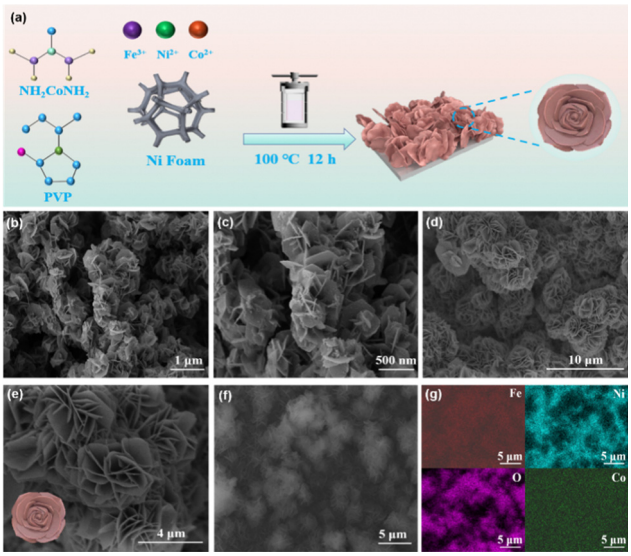

Fig. 1 (a) Scheme of the preparation of $Co_{0.2}$-FeNiOOH/NF. (b) and (c) SEM images of FeNiOOH/NF. (d) and (e) SEM images of $Co_{0.2}$-FeNiOOH/NF. (f) SEM image of $Co_{0.2}$-FeNiOOH/NF and (g) the corresponding elemental mapping.

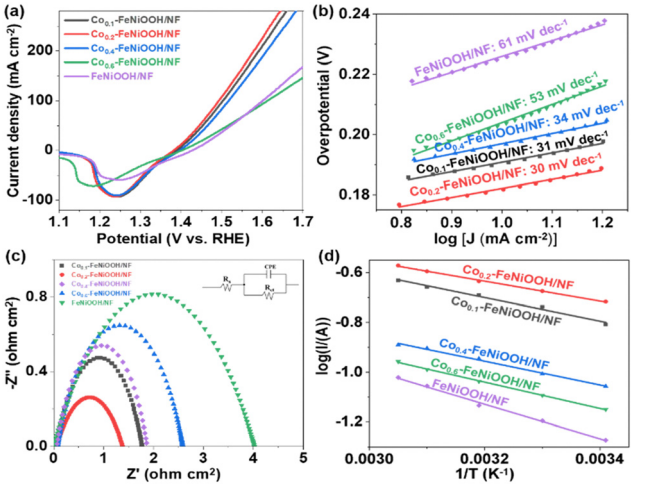

Fig. 2 (a) LSV curves of $Co_{0.1}$-FeNiOOH/NF, $Co_{0.2}$-FeNiOOH/NF, $Co_{0.4}$-FeNiOOH/NF, $Co_{0.6}$-FeNiOOH/NF and FeNiOOH/NF. (b) Tafel plots. (c) EIS plots (inset: Equivalent circuit model). (d) Arrhenius plots.

formation of the rosette-like morphology of $Co_{0.2}$-FeNiOOH/NF. The optimal $Co_{0.2}$-FeNiOOH/NF has excellent OER performance, which only needs η_{10} of 185 and 244 mV in 1 M KOH and 1 M KOH + seawater, respectively.

The composition of the synthesized electrocatalyst was determined by X-ray diffraction (XRD). The peaks at 28.2°, 42.2° and 57.2° are ascribed to NiOOH (PDF # 27-0956), while the diffraction peaks located at 21.2°, 33°, 36.7°, 41.1° and 52.9° are ascribed to FeOOH (PDF # 81-0462). In addition, the two peaks at 24°, 35.6° are ascribed to the Fe_2O_3 phase (PDF # 33-0664). After doping with Co in FeNiOOH/NF, the diffraction peaks correspond to FeOOH and NiOOH (Fig. S1, ESI†). FeNiOOH/NF exhibits a nanoflower morphology with slight stacking (Fig. 1b and c), while $Co_{0.2}$-FeNiOOH/NF has a rosette-like structure with a diameter of 3–5 μm (Fig. 1d and e). As shown in Fig. 1f and g, the element mapping reveals the even distribution of Co, Fe, Ni and O in the $Co_{0.2}$-FeNiOOH/NF.

The effect of Co doping on electrocatalytic performance in 1 M KOH was studied. As illustrated in Fig. 2a and Fig. S2 (ESI†), $Co_{0.2}$-FeNiOOH/NF shows low η_{10} and η_{50} values of 185 and 225 mV, respectively, lower than FeNiOOH/NF (222 and 292 mV), $Co_{0.1}$-FeNiOOH/NF (187 and 235 mV), $Co_{0.4}$-FeNiOOH/NF (192 and 244 mV) and $Co_{0.6}$-FeNiOOH/NF (199 and 283 mV). Compared with FeNiOOH/NF, the overpotential is significantly reduced after Co doping. From the LSV polarization curve, with the increase of Co doping, the catalytic performance of the OER increases first and then decreases, indicating that moderate Co doping in FeNiOOH/NF is conducive to improving the OER activity. The Tafel slope of 30 mV dec^{-1} for $Co_{0.2}$-FeNiOOH/NF (Fig. 2b) demonstrates a faster OER kinetic process than $Co_{0.1}$-FeNiOOH/NF (31 mV dec^{-1}), $Co_{0.4}$-FeNiOOH/NF (34 mV dec^{-1}), $Co_{0.6}$-FeNiOOH/NF (53 mV dec^{-1}) and FeNiOOH/NF (61 mV dec^{-1}). Compared with the most advanced OER electrocatalysts reported previously (Fig. S3, ESI†), $Co_{0.2}$-FeNiOOH/NF exhibits lower overpotential, such as Mo-NiOOH (310 mV),[22] Mo-FeOOH (285 mV),[23] $Ni_{0.7}Fe_{0.3}OOH$ (265 mV),[24] FeNi-CoOOH NSs/CFC (247 mV),[25] and Cu-CoOOH/CFP (234 mV).[26]

The OER kinetics was further evaluated by electrochemical impedance spectroscopy (EIS). As illustrated in Fig. 2c, the R_{ct} of $Co_{0.2}$-FeNiOOH/NF is only 1.4 Ω cm^2, which is smaller than that of $Co_{0.1}$-FeNiOOH/NF (1.8 Ω cm^2), $Co_{0.4}$-FeNiOOH/NF (1.9 Ω cm^2), $Co_{0.6}$-FeNiOOH/NF (2.6 Ω cm^2) and FeNiOOH/NF (4.0 Ω cm^2). It indicates that $Co_{0.2}$-FeNiOOH/NF has faster charge transfer and higher electrical conductivity, which will enhance its catalytic activity due to the optimized electronic structure of FeNiOOH/NF by Co doping. To investigate the intrinsic OER activity, the activation energy of these samples was calculated according to the Arrhenius formula.[27] Compared with FeNiOOH/NF (13.1 kJ mol^{-1}), $Co_{0.1}$-FeNiOOH/NF (8.8 kJ mol^{-1}), $Co_{0.4}$-FeNiOOH/NF (9.2 kJ mol^{-1}) and $Co_{0.6}$-FeNiOOH/NF (10.3 kJ mol^{-1}), $Co_{0.2}$-FeNiOOH/NF (7.5 kJ mol^{-1}) exhibits a much lower OER energy barrier (Fig. 2d and Fig. S4, ESI†), meaning that $Co_{0.2}$-FeNiOOH/NF has lower kinetic resistance. The electrochemical active surface area (ECSA) reflects effective area of the electrocatalyst participating in the electrocatalytic reaction. The ECSA of the $Co_{0.2}$-FeNiOOH/NF is 101 cm^2 (Fig. S5, ESI†), higher than $Co_{0.1}$-FeNiOOH/NF (99 cm^2) (Fig. S6, ESI†), $Co_{0.4}$-FeNiOOH/NF (96 cm^2) (Fig. S7, ESI†), $Co_{0.6}$-FeNiOOH/NF (89 cm^2) (Fig. S8, ESI†) and FeNiOOH/NF (69 cm^2) (Fig. S9, ESI†), demonstrating that the $Co_{0.2}$-FeNiOOH/NF has more catalytic available active sites. The durability of catalyst is an important factor affecting the practical application. As displayed in Fig. S10 (ESI†), the chronoamperometric test shows that $Co_{0.2}$-FeNiOOH/NF maintains good catalytic activity after 25 h continuous testing at 100 mA cm^{-2}, and the LSV polarization curve fluctuates slightly after the stability testing. The excellent OER stability can be attributed to the *in situ* growth of $Co_{0.2}$-FeNiOOH

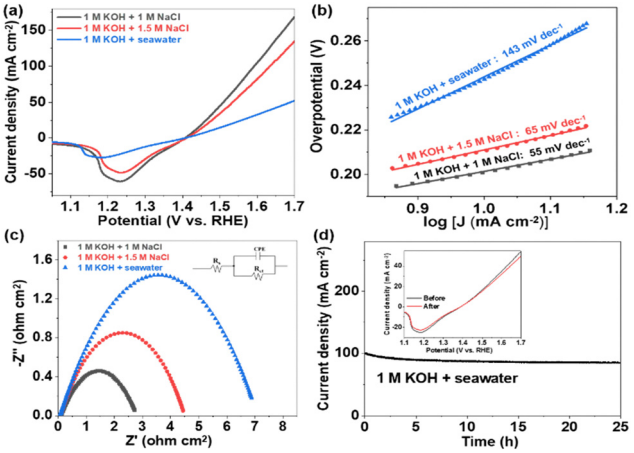

Fig. 3 (a) LSV curves of $Co_{0.2}$-FeNiOOH/NF in different electrolytes. (b) Tafel plots. (c) EIS plots (inset: Equivalent circuit model). (d) Chronoamperometric response.

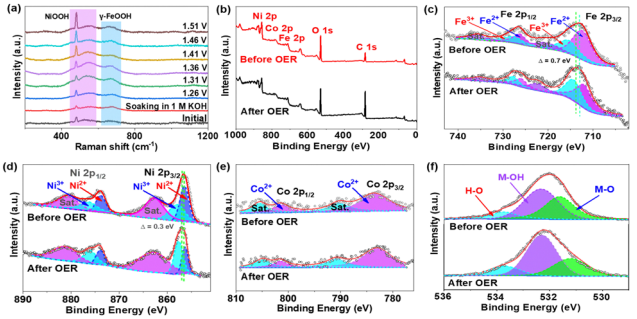

Fig. 4 (a) *In situ* Raman spectrum and, (b) XPS survey spectra of the $Co_{0.2}$-FeNiOOH/NF. XPS spectra of (c) Fe 2p, (d) Ni 2p, (e) Co 2p and (f) O 1s.

on the NF substrate, which enhances the bond strength between them.

Due to the excellent OER performance of $Co_{0.2}$-FeNiOOH/NF in an alkaline system, the OER activity of $Co_{0.2}$-FeNiOOH/NF in alkaline seawater systems was investigated. As illustrated in Fig. 3a and Fig. S11 (ESI†), the η_{10} and η_{50} values on the $Co_{0.2}$-FeNiOOH/NF in 1 M KOH + 1 M NaCl, 1 M KOH + 1.5 M NaCl, and 1 M KOH + seawater are (205 and 278 mV), (212 and 305 mV) and (244 and 455 mV), respectively. The corresponding Tafel slopes are 55 mV dec^{-1}, 65 mV dec^{-1} and 143 mV dec^{-1}, respectively (Fig. 3b). The experimental results show that $Co_{0.2}$-FeNiOOH/NF material still has a remarkable OER performance in simulated alkaline seawater and natural seawater systems. Compared with that in 1 M KOH + 1 M NaCl (2.7 Ω) and in 1 M KOH + 1.5 M NaCl (4.5 Ω), the charge transfer rate of $Co_{0.2}$-FeNiOOH/NF in 1 M KOH + seawater is lower (7.0 Ω), indicating that the presence of Cl^- anions and pollutants in seawater can hinder the charge transfer efficiency (Fig. 3c). In seawater electrolytes, the resistance to Cl^- anions and stability are important factors determining whether the catalyst is suitable for seawater electrolysis. Fig. 3d shows the stability of $Co_{0.2}$-FeNiOOH/NF in 1 M KOH + seawater at 100 mA cm^{-2}, showing that the curve fluctuates slightly and the LSV curve keeps almost constant after the stability testing, indicating that $Co_{0.2}$-FeNiOOH/NF has good stability. As illustrated in Fig. S12 (ESI†), the $Co_{0.2}$-FeNiOOH/NF has a Faradaic efficiency of 98.2% at 10 mA cm^{-2} in 1 M KOH + seawater electrolyte, indicating that most of the charge is used for the OER.

To reveal the active species of $Co_{0.2}$-FeNiOOH/NF during the OER, we performed *in situ* Raman analysis. As depicted in Fig. 4a, the $Co_{0.2}$-FeNiOOH/NF exhibits three main Raman signals. The two main Raman peaks at 480 and 558 cm^{-1} correspond to NiOOH species,[28] while the peak at 656 cm^{-1} corresponds to γ-FeOOH species.[29] With the increase of applied potential, the peak intensities gradually increase, indicating that NiOOH and γ-FeOOH are the key catalytic components for the OER. The surface chemical properties of $Co_{0.2}$-FeNiOOH/NF before and after the OER were further evaluated by XPS spectra (Fig. 4b–f). As shown in Fig. 4b, Fe, Ni, Co and O elements are detected. As illustrated in Fig. 4c and d, Fe and Ni species exist mainly in +2 and +3 valence states, respectively.[30,31] After the OER, the Fe and Ni spectra move towards higher binding energies, indicating that the metal ions were partially oxidized to higher valence states. The percentages of Fe^{3+} and Ni^{3+} contents increase significantly, indicating that more FeOOH and NiOOH species are formed during the OER. Large amounts of Fe^{3+} and Ni^{3+} have high oxidation capacity and will promote the OER, further confirming the results obtained by *in situ* Raman measurements. The Co 2p spectrum can be divided into Co $2p_{1/2}$ (801.3 eV) and Co $2p_{3/2}$ (783.1 eV), indicating the presence of Co^{2+} in $Co_{0.2}$-FeNiOOH/NF.[32] After OER, the peak intensity and position of Co 2 P spectra do not change significantly, showing that Co was doped into the material in a relatively stable form (Fig. 4e). The O 1s spectrum of $Co_{0.2}$-FeNiOOH/NF (Fig. 4f) consists of three peaks. The peaks at 531.6, 532.3 and 533.7 eV associated with M-O, M-OH (defective oxide species), and the adsorbed water, respectively.[33,34] The increased ratio of M-OH/M-O after OER test demonstrates the formation of more oxygen vacancies, which can improve the OER activity.[35] Therefore, the active species NiOOH and γ-FeOOH play a major role in the OER, since the high valence metal ions have strong oxidation capacity. The introduction of Co and the formation of oxygen vacancies further regulate the electronic structure and optimize the adsorption energy of intermediates, thus promoting the OER. According to the XPS semi-quantitative formula of relative atomic concentration on the catalyst surface $\left(\frac{n_i}{n_j} = \frac{I_i}{I_j} \times \frac{\sigma_j}{\sigma_i} \times \frac{E_{kj}^{0.5}}{E_{ki}^{0.5}}\right)$, where n is the number of surface atoms, I is the peak area integral, σ is the photoionization cross section of the corresponding energy level of an element, E_k is the kinetic energy of photoelectrons; the atomic concentration ratio of Ni, Fe and Co elements is calculated to be about 1 : 1 : 0.15, meaning that Co was successfully doped into FeNiOOH/NF. The morphology of $Co_{0.2}$-FeNiOOH/NF after the OER test was further observed through SEM. As shown in Fig. S13 (ESI†), the rosette-like structure of the material can be well maintained, indicating that $Co_{0.2}$-FeNiOOH/NF has good structural stability during the OER.

To explore the application potential of $Co_{0.2}$-FeNiOOH/NF in overall water splitting, we constructed a two-electrode system with $Co_{0.2}$-FeNiOOH/NF as the anode and Pt/C as the cathode. As depicted in Fig. S14a (ESI†), the $Co_{0.2}$-FeNiOOH/NF‖Pt/C electrolyzer requires 1.53 V to reach 10 mA cm^{-2}, which is much lower than that of the IrO_2/NF‖Pt/C electrolyzer (1.65 V). In addition, no significant degradation occurs after 25 h of continuous operation (Fig. S14b, ESI†). The above results indicate that $Co_{0.2}$-FeNiOOH/NF is a promising OER electrocatalyst in practical applications.

In conclusion, we successfully synthesized a rosette-like $Co_{0.2}$-FeNiOOH/NF through one-step solvothermal method for efficient seawater oxidation. The $Co_{0.2}$-FeNiOOH/NF exhibited superior OER performance in 1 M KOH and 1 M KOH + seawater, with an η_{10} of 185 and 244 mV, respectively, and excellent stability. Moreover, by coupling with Pt/C, the $Co_{0.2}$-FeNiOOH/NF‖Pt/C cell only needs a low voltage of 1.53 V to deliver 10 mA cm^{-2}. The remarkable OER activity of $Co_{0.2}$-FeNiOOH/NF is chiefly ascribed to the fact that the introduction of Co regulates the morphology to be rosette-like, which provides abundant active sites for the reaction, promotes charge transfer, and speeds up the OER.

This work was supported by the National Natural Science Foundation of China (No. 22075099), the Natural Science Foundation of Jilin Province (No. 20220101051JC), and the Basic Science Research Project of Heilongjiang Provincial University (No. 145109109).

Conflicts of interest

There are no conflicts to declare.

References

1 Y. Zhou, Y. S. Wu, D. X. Guo, J. L. Li, G. H. Dong, D. F. Chai, X. Yang, S. S. Fu and G. Z. Sui, *Mater. Chem. Front*, 2023, **7**, 306–314.
2 N. K. Shrestha, S. A. Patil, A. I. Inamdar, S. Park, S. Yeon, G. Shin, S. Cho, H. Kim and H. Im, *Dalton Trans.*, 2022, **51**, 8994–9006.
3 T. M. Tang, Y. Wang, J. Y. Han, Q. Q. Zhang, X. Bai, X. D. Niu, Z. L. Wang and J. Q. Guan, *Chin. J. Catal.*, 2023, **46**, 48–55.
4 Y. Y. Liu, D. J. Zhou, T. Y. Deng, G. L. He, A. B. Chen, X. M. Sun, Y. H. Yang and P. Miao, *ChemSusChem*, 2021, **14**, 5359–5383.
5 N. K. Shrestha, S. A. Patil, S. Cho, Y. Jo, H. Kim and H. Im, *J. Mater. Chem. A*, 2020, **8**, 24408–24418.
6 T. M. Tang, Z. L. Wang and J. Q. Guan, *Coord. Chem. Rev.*, 2023, **492**, 215288.
7 A. N. Angelakis, M. Valipour, K. H. Choo, A. T. Ahmed, A. Baba, R. Kumar, G. S. Toor and Z. W. Wang, *Water*, 2021, **13**, 2222.
8 S. Dresp, T. N. Thanh, M. Klingenhof, S. Bruckner, P. Hauke and P. Strasser, *Energy Environ. Sci.*, 2020, **13**, 1725–1729.
9 L. Yu, Q. Zhu, S. W. Song, B. McElhenny, D. Z. Wang, C. Z. Wu, Z. J. Qin, J. M. Bao, Y. Yu, S. Chen and Z. F. Ren, *Nat. Commun.*, 2019, **10**, 5106.
10 C. Huang, T. Ouyang, Y. Zou, N. Li and Z. Q. Liu, *J. Mater. Chem. A*, 2018, **6**, 7420–7427.
11 N. K. Shrestha, S. A. Patil, J. Han, S. Cho, A. I. Inamdar, H. Kim and H. Im, *J. Mater. Chem. A*, 2022, **10**, 8989–9000.
12 J. Y. Han and J. Q. Guan, *Nano Res.*, 2023, **16**, 1913–1966.
13 Z. L. Zhu, C. X. Xu, Y. C. Wang, L. Wang, Z. Chang, Z. W. Fang, X. T. Liu and J. G. Cheng, *J. Alloys Compd.*, 2022, **894**, 162393.
14 Z. H. Liu, J. H. Hu, S. Li, C. Lu, K. Feng, S. F. Wang and J. Zhong, *Appl. Surf. Sci.*, 2023, **631**, 157590.
15 X. X. Yu, Z. Y. Yu, X. L. Zhang, P. Li, B. Sun, X. C. Gao, K. Yan, H. Liu, Y. Duan, M. R. Gao, G. X. Wang and S. H. Yu, *Nano Energy*, 2020, **71**, 104652.
16 D. X. Liang, J. X. Mao, P. Liu, J. W. Li, J. Y. Yan and W. B. Song, *Int. J. Hydrogen Energy*, 2020, **45**, 27047–27055.
17 Z. J. Zhu, H. J. Yin, C. T. He, M. Al-Mamun, P. R. Liu, L. X. Jiang, Y. Zhao, Y. Wang, H. G. Yang, Z. Y. Tang, D. Wang, X. M. Chen and H. J. Zhao, *Adv. Mater.*, 2018, **30**, 1801171.
18 S. R. Ede and Z. P. Luo, *J. Mater. Chem. A*, 2021, **9**, 20131–20163.
19 N. K. Shrestha, S. A. Patil, A. S. Salunke, A. I. Inamdar and H. Im, *J. Mater. Chem. A*, 2023, **11**, 14870–14877.
20 L. Ding, K. Li, Z. Q. Xie, G. Q. Yang, S. L. Yu, W. T. Wang, H. R. Yu, J. Baxter, H. M. Meyer, D. A. Cullen and F. Y. Zhang, *ACS Appl. Mater. Interfaces*, 2021, **13**, 20070–20080.
21 C. Lan, H. P. Xie, Y. F. Wu, B. Chen and T. Liu, *Energy Fuels*, 2022, **36**, 2910–2917.
22 Y. S. Jin, S. L. Huang, X. Yue, C. Shu and P. K. Shen, *Int. J. Hydrogen Energy*, 2018, **43**, 12140–12145.
23 Z. C. Jia, X. Lyu, M. S. Zhao, J. A. Dang, L. E. Zhu, X. W. Guo, X. B. Wang, Z. Y. Bai and L. Yang, *Chem. – Asian J.*, 2023, **18**, e202201305.
24 F. Ahmad, A. Ali and J. Q. Qin, *Results Chem.*, 2023, **5**, 100808.
25 N. Ma, C. C. Gong, H. A. Xie, C. S. Shi, J. W. Sha, C. N. He, F. He, N. Q. Zhao and E. Z. Liu, *Int. J. Hydrogen Energy*, 2022, **47**, 29762–29770.
26 L. Yan, B. Zhang, Z. G. Liu and J. L. Zhu, *Chem. Eng. J.*, 2021, **405**, 126198.
27 M. Y. Shi, T. M. Tang, L. Y. Xiao, J. Y. Han, X. Bai, Y. H. Sun, S. Y. Chen, J. R. Sun, Y. Y. Ma and J. Q. Guan, *Chem. Commun.*, 2023, **59**, 11971–11974.
28 X. H. Liu and J. Wu, *Electrochim. Acta*, 2019, **320**, 134577.
29 M. K. Nieuwoudt, J. D. Comins and I. Cukrowski, *J. Raman Spectrosc.*, 2011, **42**, 1335–1339.
30 T. Yamashita and P. Hayes, *Appl. Surf. Sci.*, 2008, **254**, 2441–2449.
31 O. Allahdin, S. C. Dehou, M. Wartel, P. Recourt, M. Trentesaux, J. Mabingui and A. Boughriet, *Chem. Eng. Res. Des.*, 2013, **91**, 2732–2742.
32 M. Yue, X. He, S. J. Sun, Y. T. Sun, M. S. Hamdy, M. Benaissa, A. A. M. Salih, J. Liu and X. P. Sun, *Nano Res.*, 2023, DOI: 10.1007/s12274-023-6002-6.
33 X. Bai, J. Y. Han, X. D. Niu and J. Q. Guan, *Nano Res.*, 2023, **16**, 10796–10802.
34 H. L. Wang, Z. F. Zhao, Z. K. Xu, L. Li and S. Y. Lin, *Dalton Trans.*, 2023, **52**, 1113–1121.
35 X. Chen, Q. C. Wang, Y. W. Cheng, H. L. Xing, J. Z. Li, X. J. Zhu, L. B. Ma, Y. T. Li and D. M. Liu, *Adv. Funct. Mater.*, 2022, **32**, 2112674.

